A New Balanced-to-Unbalanced Filtering Power Divider With Dual Controllable Passbands and Enhanced In-Band Common-Mode Suppression

Feng Huang, Jianpeng Wang, Jiasheng Hong, *Fellow, IEEE*, and Wen Wu, *Senior Member, IEEE*

***Abstract*— A new microstrip balanced-to-unbalanced power divider with dual bandpass filtering response is presented in this paper. The generalized mixed-mode scattering matrix for the filtering balanced-to-unbalanced power divider is derived to guide the design. Differential-mode (DM) dual-band filtering response is analyzed under the odd-mode excitation to show that the frequency ratio ($k = f_2/f_1$) and bandwidth of these two passbands could be flexibly controlled. For the even-mode excitation, two intrinsic transmission zeros generated by additional open-ended stub are introduced, aiming to achieve the enhancement of in-band common-mode (CM) suppression. In addition, good in-band isolation and port matching are realized by introducing a grounded resistor. To validate the design concept, two prototypes centering at 1 and 2.5 GHz ($k = 2.5$), as well as 0.76 and 2.75 GHz ($k = 3.62$) are implemented following the given design procedure. Tested results of the two fabricated circuits, well agreeing with the simulated ones, exhibit high performances in terms of DM response, in-band CM suppression, port-to-port isolation, and port matching.**

***Index Terms*— Balanced-to-unbalanced, common-mode (CM) suppression, dual passband, filtering response, power divider.**

I. Introduction

THE bandpass filter and the power divider are two essential passive components in modern wireless communication systems. Typically, an excessive area would be occupied when these two devices coexist in the same radio frequency (RF) front end. To tackle this problem, one effective approach for size miniaturization is to integrate these two devices into a single component, i.e., the filtering power divider, possessing the functions of power splitting/combining, and frequency selectivity simultaneously. During the past decade, many works dealing with this multifunction embedded component have been reported in the open literature, and thus a wide variety of circuit implementations are available today with different design methods [1]–[8]. Among them, the representative works include combining the power divider with the filter directly [1], [2], replacing two quarter-wavelength transmission line with the filtering units [3]–[5], and introducing three-line coupled structures [6]–[8]. Note that all the aforementioned works are focused on the single-ended filtering power dividers.

On the other hand, balanced circuits, such as balanced filter [9] and balanced diplexer [10], have been widely utilized due to their high common-mode (CM) rejection and immunity against noise. Recently, the differential technology has been applied to design balanced power dividers as well [11]–[15], which can be served as a good candidate in a fully balanced RF front end. In addition, a balanced power divider with bandpass filtering response is presented in [16] based on a ring structure. Other balanced-to-balanced filtering power dividers using microstrip [17] and SIW [18] technologies have also been reported.

Compared with the above-mentioned fully balanced power divider, the balanced-to-unbalanced filtering power divider exhibits more flexibility to integrate balanced circuits with single-ended ones. Fig. 1 shows a typical application case of such a device in RF front-end transceivers for the dual-band operation. As is shown, in the transmitting path, the magnified differential signal from the balanced power amplifier can be converted into two-way dual-band single-ended signals by the balanced-to-unbalanced filtering power divider, and then delivered to the antenna array. While for the receiving path, the single-ended signals from the antenna array are fed back to the balanced low-noise amplifier in a differential type, again through the proposed power divider.

In order to realize the functions of balanced-to-unbalanced signal conversion and dual-band filtering performance, a conventional solution by directly cascading balun, power divider, and dual-band filters is shown in Fig. 2(a). Obviously, this approach suffers from enlarged overall size and high insertion loss. Thus, a trend of integration design shown in Fig. 2(b) is

Manuscript received March 11, 2018; revised July 31, 2018; accepted October 31, 2018. This work was supported in part by the National Natural Science Foundation of China under Grant 61771247, in part by the State Key Laboratory of Millimeter Waves under Grant K201921, and in part by the Postgraduate Research and Practice Innovation Program of Jiangsu Province under Grant KYCX18_0421. *(Corresponding author: Jianpeng Wang.)*

F. Huang and J. Wang are with the Ministerial Key Laboratory of JGMT, Nanjing University of Science and Technology, Nanjing 210094, China, and also with the State Key Laboratory of Millimeter Waves of China, Nanjing 210096, China (e-mail: jianpeng_wang@126.com).

J. Hong is with the Department of Electrical, Electronic and Computer Engineering, School of Engineering and Physical Sciences, Heriot-Watt University, Edinburgh EH14 4AS, U.K. (e-mail: j.hong@hw.ac.uk).

W. Wu is with the Ministerial Key Laboratory of JGMT, Nanjing University of Science and Technology, Nanjing 210094, China.

Color versions of one or more of the figures in this paper are available online at http://ieeexplore.ieee.org.

Digital Object Identifier 10.1109/TMTT.2018.2883100

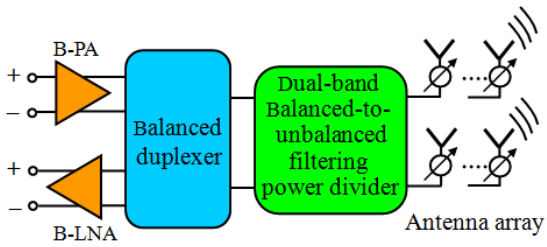

Fig. 1. Proposed power divider for a dual-passband antenna array application.

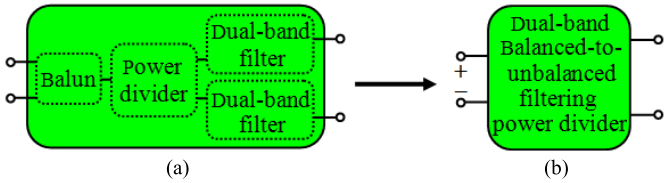

Fig. 2. Schematics of two dual-band balanced-to-unbalanced power dividers with filtering response. (a) Traditional one with cascaded balun, power divider, and dual-band filters. (b) Proposed one with one single circuitry.

meaningful for size reduction and impedance matching. Although balanced-to-unbalanced power dividers implemented by using a four-wire coupled-line and T-shaped structures [19], coupled-lines [20], [21], transmission lines [22]–[24] have been reported, none of these works can block the input signal outside their desired operating bands. Recently, the authors have proposed two balanced-to-unbalanced power dividers with filtering response on branch lines and several stubs [25]. In addition, coupled-line based balanced-to-unbalanced filtering power dividers have been also developed in [26]. Despite the fact that wideband filtering response with high selectivity is achieved, the CM suppression and single-ended port responses are not ideal within the whole wide passband, thus needing to be further improved.

To the best of our knowledge, only limited work has been carried out on the dual-band balanced-type filtering power dividers. In [27], a differential filtering power divider with dual passbands is designed without addressing the isolation between output ports. Another dual-band balanced-to-unbalanced filtering power divider based on coupled ring resonators [28] cannot control its dual passbands flexibly and is just suitable for the design with two closely located passbands.

The main motivation of this paper is to present a new codesign of balanced-to-unbalanced filtering power divider with dual controllable passbands. This power divider not only can simultaneously convert the input differential signals into single-ended ones at two designated frequencies with equal power division and bandpass-filtering response but also have the advantage of rejecting the undesired in-band CM signals. Theoretical analysis, closed-form equations, as well as detailed design procedure are presented to guide the proposed design. Finally, two practical prototypes with different frequency ratios of $k = f_2/f_1 = 2.5$ and 3.62 are designed, fabricated, and measured for experimental validation. Both simulated and measured results of the implemented circuits are recorded and good agreement between them is obtained. Overall, compared with state-of-the art primary advantages of the proposed power divider reported in this paper are summarized as follows.

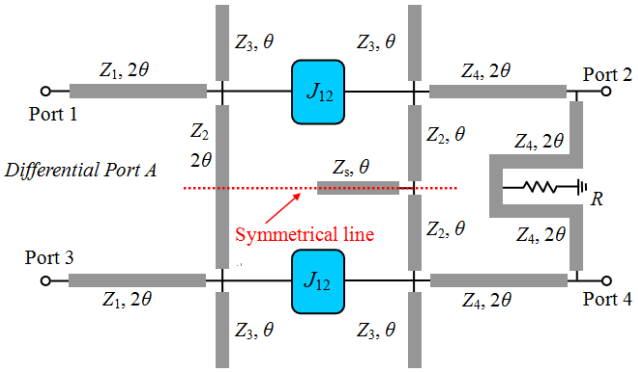

Fig. 3. Schematic of the proposed dual-band balanced-to-unbalanced filtering power divider.

1) *Single Circuitry:* The proposal is a highly integrated design, which can provide multifunctions of balanced-to-unbalanced signal conversion, power division, frequency selectivity, dual-band operation, port-to-port isolation, and CM suppression simultaneously with only one single component.
2) *Concise Analysis:* The generalized mixed-mode scattering matrix is at first derived and found only related to the individual odd- and even-mode S-parameters, thus facilitating the proposed design by using even–odd-mode method.
3) *Flexible Band Ratio:* The proposed dual-band admittance inverter structures could operate under the condition of either the band ratio, $k < 3$ or $k > 3$, thus ensuring the filtering power divider works at two passbands with great flexibility.
4) *Improved Performance:* The desired dual-band filtering response is effectively obtained under the odd-mode excitation, while the in-band CM suppression is enhanced significantly due to a pair of introduced transmission zeros.

II. Theoretical Analysis

The circuit model of the proposed dual-band balanced-to-unbalanced filtering power divider is depicted in Fig. 3. It has one balanced or differential input port A, which is formed up by physical ports 1 and 3, and two single-ended output ports 2 and 4. Two step-impedance resonators (Z_3, θ) and $(Z_2, 2\theta)$ are coupled each other by a pair of dual-band admittance inverters J_{12} to facilitate the basic dual-band responses. Four extended transmission lines $(Z_1, 2\theta)$ and $(Z_4, 2\theta)$ at each port are employed for dual-band impedance matching. Note that the open-circuited stub (Z_s, θ) loading on the symmetrical line is introduced to enhance the CM suppression. In addition, a grounded resistor R is added on the middle of the transmission line $(Z_4, 4\theta)$ to achieve good isolation and port matching.

A. Generalized Mixed-Mode Scattering Matrix Analysis

First, let us consider the standard scattering matrix $[S_{\text{std}}]$ of the proposed balanced-to-unbalanced filtering power divider in Fig. 1. Since this configuration can be deemed as a

symmetrical and reciprocal four-port network, $[S_{\text{std}}]$ could be defined as

$$[S_{\text{std}}]=\begin{bmatrix} S_{11} & S_{12} & S_{13} & S_{14} \\ S_{21} & S_{22} & S_{23} & S_{24} \\ S_{31} & S_{32} & S_{33} & S_{34} \\ S_{41} & S_{42} & S_{43} & S_{44} \end{bmatrix}=\begin{bmatrix} a & b & c & d \\ b & e & d & f \\ c & d & a & b \\ d & f & b & e \end{bmatrix}. \quad (1)$$

On the other hand, with reference to the port assignment (balanced port A and two single-ended ports 2 and 4) shown in Fig. 3, the required mixed-mode scattering matrix $[S_{\text{mm}}]$ is expressed as below according to [29]

$$[S_{\text{mm}}]=\begin{bmatrix} S_{\text{ddAA}} & S_{\text{dcAA}} & S_{\text{dsA2}} & S_{\text{dsA4}} \\ S_{\text{cdAA}} & S_{\text{ccAA}} & S_{\text{csA2}} & S_{\text{csA4}} \\ S_{\text{sd2A}} & S_{\text{sc2A}} & S_{\text{ss22}} & S_{\text{ss24}} \\ S_{\text{sd4A}} & S_{\text{sc4A}} & S_{\text{ss42}} & S_{\text{ss44}} \end{bmatrix} \quad (2)$$

where the subscripts d, c, and s represent the differential mode (DM), CM, and single-ended port, respectively. By taking advantage of the matrix transformation technique provided in [30], the mixed-mode scattering matrix $[S_{\text{mm}}]$ is attained as (3a), shown at the bottom of this page. Moreover, according to [31], the individual odd-/even-mode S-parameters can be indicated as

$$S^o_{i,j} = S_{i,j} - S_{i,n+j} \quad (4a)$$

$$S^e_{i,j} = S_{i,j} + S_{i,n+j} \quad (4b)$$

where symbols o and e correspond to the odd- and even-mode equivalent subcircuits i, $j = 1, 2, n = 2$, and $S_{i,j}$ and $S_{i,n+j}$ stand for the internal elements in the standard matrix $[S_{\text{std}}]$.

Consequently, by substituting (4) into (3a), the generalized mixed-mode scattering matrix $[S_{\text{mm}}]$ can be simplified into (3b), shown at the bottom of this page. As we can see, all the mixed-mode S-parameters are related to the individual odd-/even-mode S-parameters. In this context, it is very convenient to characterize the proposed new design in terms of the desired DM dual-band filtering response, the CM suppression, the port-to-port isolation, as well as the port matching condition by the well-known even–odd-mode method.

B. Odd-Mode Analysis

When an odd-mode excitation is applied to ports 1 and 3, the plane along the symmetrical line can be deemed as an electrical wall and the resultant odd-mode equivalent circuit is presented in Fig. 4(a), which is equivalent to a two-port second-order dual-band filter. The operating frequencies of two passbands are determined by the dual-passband resonator consisting of two impedance sections of Z_2 and Z_3 with identical electrical length of θ. The first two resonant frequencies are given by [32] as

$$f_1 = \frac{2f_0}{\pi}\arctan\sqrt{R_z} \quad (5a)$$

$$f_2 = \frac{2f_0}{\pi}\left(\pi - \arctan\sqrt{R_z}\right) \quad (5b)$$

where f_0 is the central frequency of $\theta = \pi/2$ and R_z is defined as the impedance ratio of Z_3/Z_2. Thus, the frequency ratio of two passbands is given by

$$k = \frac{f_2}{f_1} = \frac{\pi - \arctan\sqrt{R_z}}{\arctan\sqrt{R_z}}. \quad (6)$$

The bandwidth control is discussed next. As shown in Fig. 4(b), two types of dual-band J-inverters consisting of

$$[S_{\text{mm}}] = \begin{bmatrix} \frac{S_{11}-S_{13}-S_{31}+S_{33}}{2} & \frac{S_{11}+S_{13}-S_{31}-S_{33}}{2} & \frac{S_{12}-S_{32}}{\sqrt{2}} & \frac{S_{14}-S_{34}}{\sqrt{2}} \\ \frac{S_{11}+S_{13}-S_{31}-S_{33}}{2} & \frac{S_{11}+S_{13}+S_{31}+S_{33}}{2} & \frac{S_{12}+S_{32}}{\sqrt{2}} & \frac{S_{14}+S_{34}}{\sqrt{2}} \\ \frac{S_{21}-S_{23}}{\sqrt{2}} & \frac{S_{21}+S_{23}}{\sqrt{2}} & S_{22} & S_{24} \\ \frac{S_{41}-S_{43}}{\sqrt{2}} & \frac{S_{41}+S_{43}}{\sqrt{2}} & S_{42} & S_{44} \end{bmatrix}$$

$$= \begin{bmatrix} a-c & 0 & \frac{b-d}{\sqrt{2}} & -\frac{b-d}{\sqrt{2}} \\ 0 & a+c & \frac{b+d}{\sqrt{2}} & \frac{b+d}{\sqrt{2}} \\ \frac{b-d}{\sqrt{2}} & \frac{b+d}{\sqrt{2}} & e & f \\ -\frac{b-d}{\sqrt{2}} & \frac{b+d}{\sqrt{2}} & f & e \end{bmatrix} \quad (3a)$$

$$[S_{\text{mm}}] = \begin{bmatrix} S^o_{11} & 0 & \frac{1}{\sqrt{2}}S^o_{21} & -\frac{1}{\sqrt{2}}S^o_{21} \\ 0 & S^e_{11} & \frac{1}{\sqrt{2}}S^e_{21} & \frac{1}{\sqrt{2}}S^e_{21} \\ \frac{1}{\sqrt{2}}S^o_{21} & \frac{1}{\sqrt{2}}S^e_{21} & \frac{1}{2}\left(S^e_{22}+S^o_{22}\right) & \frac{1}{2}\left(S^e_{22}-S^o_{22}\right) \\ -\frac{1}{\sqrt{2}}S^o_{21} & \frac{1}{\sqrt{2}}S^e_{21} & \frac{1}{2}\left(S^e_{22}-S^o_{22}\right) & \frac{1}{2}\left(S^e_{22}+S^o_{22}\right) \end{bmatrix} \quad (3b)$$

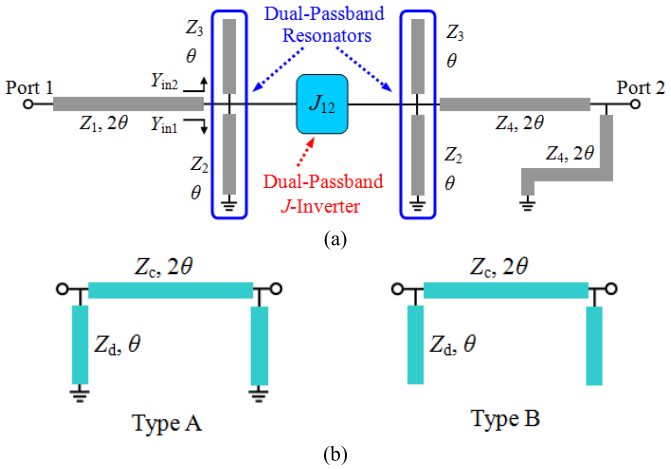

Fig. 4. (a) Half a bisection of equivalent circuit under odd-mode excitation. (b) Two types of the proposed dual-band admittance inverters.

transmission line $(Z_c, 2\theta)$ and short or open stubs (Z_d, θ) are adopted herein to obtain the desired internal coupling coefficients between two resonators.

In order to ensure type A and B admittance inverters are suitable for dual-band operation, the total ABCD parameters of these two configurations should be equal to an ideal admittance inverter at the two designated frequencies of f_1 and f_2, illustrated as follows:

$$\begin{bmatrix} 1 & 0 \\ -j\dfrac{\cot\theta}{Z_d} & 1 \end{bmatrix} \begin{bmatrix} \cos 2\theta & jZ_c \sin 2\theta \\ j\dfrac{\sin 2\theta}{Z_c} & \cos 2\theta \end{bmatrix} \begin{bmatrix} 1 & 0 \\ -j\dfrac{\cot\theta}{Z_d} & 1 \end{bmatrix} = \begin{bmatrix} 0 & j\dfrac{1}{J_{12}} \\ jJ_{12} & 0 \end{bmatrix} \tag{7a}$$

$$\begin{bmatrix} 1 & 0 \\ j\dfrac{\tan\theta}{Z_d} & 1 \end{bmatrix} \begin{bmatrix} \cos 2\theta & jZ_c \sin 2\theta \\ j\dfrac{\sin 2\theta}{Z_c} & \cos 2\theta \end{bmatrix} \begin{bmatrix} 1 & 0 \\ j\dfrac{\tan\theta}{Z_d} & 1 \end{bmatrix} = \begin{bmatrix} 0 & j\dfrac{1}{J_{12}} \\ jJ_{12} & 0 \end{bmatrix}. \tag{7b}$$

After theoretical simplification, the following design equations are derived:

$$Z_c = \frac{1+R_z}{2\sqrt{R_z}J_{12}} \qquad Z_d = \frac{2Z_c}{R_z - 1} \tag{8a}$$

$$Z_c = \frac{1+R_z}{2\sqrt{R_z}J_{12}} \qquad Z_d = \frac{2R_z Z_c}{1 - R_z}. \tag{8b}$$

Evidently, the impedance ratio R_z must be greater than 1 in (8a) for type A and smaller than 1 in (8b) for type B. This means, according to (6), that the type A dual-band admittance inverter is applicable under the condition of frequency ratio $k < 3$, while the type B inverter is suitable to operate for frequency ratio $k > 3$.

As detailed in [33], the required coupling degrees M_{12} and M'_{12} can be established as

$$M_{12} = \frac{\mathrm{FBW}_1}{\sqrt{g_1 g_2}} = \frac{J_{12}}{b_1} \tag{9a}$$

$$M'_{12} = \frac{\mathrm{FBW}_2}{\sqrt{g_1 g_2}} = \frac{J_{12}}{b_2} \tag{9b}$$

where FBW_i $(i = 1, 2)$ is the fractional bandwidth of the first or second passband, g_i $(i = 1, 2)$ is normalized element in the low-pass filter prototype, and b_i $(i = 1, 2)$ is the susceptance slope parameter [33], which can be calculated by

$$b_i = \frac{f}{2}\left.\frac{d[\mathrm{Im}(Y_{\mathrm{in1}} + Y_{\mathrm{in2}})]}{df}\right|_{f=f_1, f_2} \tag{10}$$

where Y_{in1} and Y_{in2} are input admittances as labeled in Fig. 4 (a).

The expression for the two susceptance slope parameters at each operating frequency can be simplified as

$$b_1 = \frac{1}{2Z_3}\theta_1 \sec^2\theta_1 + \frac{1}{2Z_2}\theta_1 \csc^2\theta_1 \tag{11a}$$

$$b_2 = \frac{\pi}{\theta_1}b_1 - b_1. \tag{11b}$$

Combining with (6), (8), (9), and (11), we have obtained the following identities:

$$\frac{\mathrm{FBW}_1}{\mathrm{FBW}_2} = \frac{\mathrm{ABW}_1/f_1}{\mathrm{ABW}_2/f_2} = \frac{f_2}{f_1} \tag{12a}$$

$$\mathrm{FBW}_1 = \frac{(1+R_z)Z_3\sqrt{g_1 g_2}}{\sqrt{R_z}Z_c(\theta_1 \sec^2\theta_1 + R_z\theta_1 \csc^2\theta_1)}. \tag{12b}$$

From (12a), we can find that the absolute bandwidth (ABW) of both passbands are always kept identical, which makes it very suitable for the application requiring dual constant absolute bandwidths. Moreover, (12b) reveals the relationship between FBW_1 and the impedance Z_c under different values of Z_3 and R_z. In other words, the bandwidths of our design can be controlled flexibly with different frequency ratios.

Furthermore, the circuit parameter Z_c can be easily determined according to the specific design requirement of the given FBWs once the dual-passband resonator is confirmed.

As for the external quality factors Q_{ei} [33] $(i = 1, 2)$, they can be derived as

$$Q_{\mathrm{in}i} = Q_{\mathrm{out}i} = Q_{ei} = \frac{g_0 g_1}{\mathrm{FBW}_i}. \tag{13}$$

In our design, the dual-band impedance transformers $(Z_1, 2\theta)$ are tapped to the dual-band resonator in order to satisfy the input Q-factors. Analogously, as discussed in [34], the electrical lengths of the dual-band impedance transformers are set as 2θ, and the characteristic impedance Z_1 is calculated as

$$Z_1 = \left.\sqrt{Z_0\frac{Q_{ei}}{b_i}}\right|_{i=1,2}. \tag{14}$$

After Z_1 is decided, a fine tuning of Z_4 is required to ensure that the output Q-factors coincide with the derived ones as given in (13).

Till now, based on the odd-mode equivalent circuit shown in Fig. 4(a), the DM responses including operating frequencies, bandwidths, as well as the external quality factors are well analyzed, which is very meaningful to guide our design. Next, the approach of achieving enhanced CM suppression, good port matching and isolation for dual passbands will be described in detail in Section II-C.

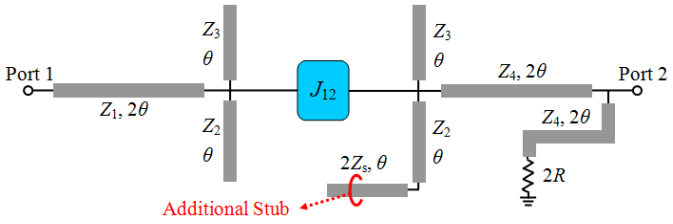

Fig. 5. Half a bisection of equivalent circuit under even-mode excitation.

C. Even-Mode Analysis

Under the even-mode excitation, the symmetrical plane can be viewed as a magnetic wall, and the even-mode equivalent circuit is shown in Fig. 5, which is utilized to realize improved CM suppression, good isolation, and port matching.

As we can observe, the additional stub, just loaded in the symmetrical plane, is introduced to generate extra transmission zeros for the enhancement of CM rejection without interfering the DM response. By analyzing this CM equivalent circuit, the first three transmission zeros are obtained as

$$f_{z1} = \frac{2f_0}{\pi}\arctan\sqrt{\frac{2Z_s}{Z_2}} \tag{15a}$$

$$f_{z2} = f_0 \tag{15b}$$

$$f_{z3} = \frac{2f_0}{\pi}\left(\pi - \arctan\sqrt{\frac{2Z_s}{Z_2}}\right) \tag{15c}$$

where Z_s is the characteristic impedance of the loaded stub.

For direct demonstration, a set of CM transmission coefficients with and without the loaded stub are plotted in Fig. 6. As expected, the CM signal can be greatly rejected at f_{z1} and f_{z3} with the help of this loaded stub. Moreover, as illustrated in Fig. 6, these two transmission zeros f_{z1} and f_{z3} can be adjusted flexibly by varying the value of Z_s, which indicates that the in-band CM suppression could be enhanced a lot by relocating transmission zeros f_{z1} and f_{z3} at the DM resonant frequencies.

Next, it is to show how a proper grounded resistor R can be found to realize high performance of port matching and isolation. According to (3b), the isolation and port-matching condition could be characterized by

$$S_{ss24} = 0.5\left(S_{22}^e - S_{22}^o\right) \tag{16a}$$

$$S_{ss22} = 0.5\left(S_{22}^e + S_{22}^o\right). \tag{16b}$$

In order to achieve good isolation and port matching, the following relations should be complied in both two designed passbands:

$$\mathrm{Re}\left(S_{22}^o\right) = \mathrm{Im}\left(S_{22}^o\right) = 0 \tag{17a}$$

$$\mathrm{Re}\left(S_{22}^e\right) = \mathrm{Im}\left(S_{22}^e\right) = 0 \tag{17b}$$

where Re and Im represent the real part and imaginary part, respectively.

Note that (17a) would be established without doubt when the desired DM filtering response is determined. That is to say, we have to select appropriate parameters to satisfy (17b). Since the characteristic impedance of the loaded stub Z_s is determined by the CM performance, the isolation and port matching are mainly related to the resistor R. In this context, by varying the value of R, we can find an optimal value to make (17b) tenable to the greatest extent for good isolation and port matching performance.

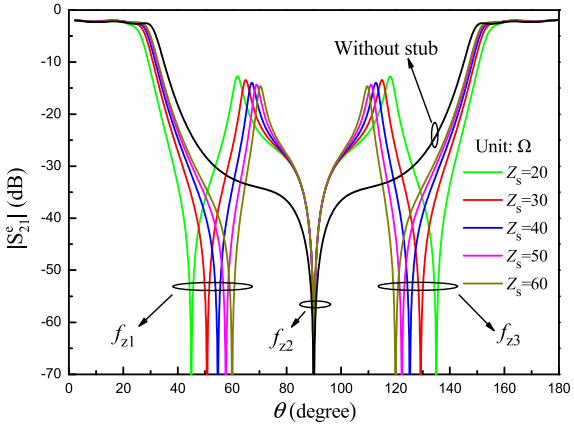

Fig. 6. Set of CM transmission coefficients under the DM frequency ratio of $k = 2.5$.

D. Design Procedure

To clarify the design of the proposed dual-band balanced-to-unbalanced filtering power divider, the detailed design procedure is described as follows.

1) *Design of the DM Dual-Band Filtering Response:* First, selecting proper type of the dual-band admittance inverter based on two given central frequencies f_1 and f_2. Then, determining the impedance Z_c and Z_d to obtain the desired FBWs according to (8) and (12). Finally, calculating Z_1 using (14) to achieve the expected Q-factors at input port, and then selecting proper Z_4 for output Q-factors.
2) *Enhancement of the CM Suppression:* Based on (15), by means of tuning the impedance of the loaded stub on the symmetrical plane, enhanced in-band CM rejection can be acquired with the relocation of the transmission zeros f_{z1} and f_{z3} in the DM dual passbands.
3) *Implementation of In-Band Single-Ended Port Responses:* Since in-band port matching and isolation are related to the resistor R based on the above analysis, choosing proper value of R to satisfy (17b) as far as possible.
4) *Optimization Process of the Design Circuit:* Embedding the short or open stubs (Z_d, θ) in the proposed dual-band admittance inverters into the dual-band resonators for size compactness, and executing the final optimization of the realized entire circuit layout relying on the commercial EM simulator.

III. Experiments, Measurements, and Comparison

In this section, two prototypes have been implemented on Rogers RO4003C substrate ($\varepsilon_r = 3.55$, $\tan\delta = 0.0027$) with a thickness of 0.508 mm to validate the design theory. Simulation is accomplished by the commercial full-wave simulator ANSOFT HFSS, while the measurement is carried out in the Agilent N5244A four-port vector network analyzer.

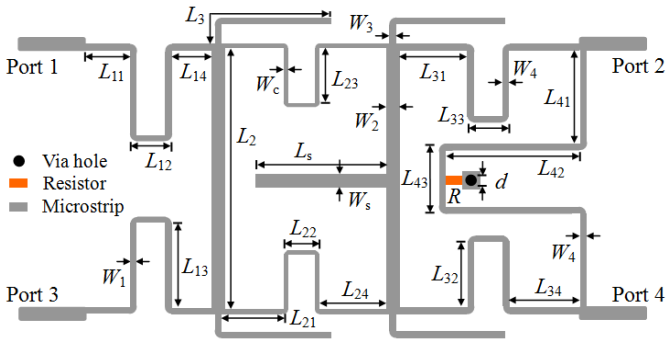

Fig. 7. Layout of Prototype I with dimensions denoted. [$L_{11} = 7.57$, $L_{12} = 6.26$, $L_{13} = 15$, $L_{14} = 6.82$, $L_{21} = 12.01$, $L_{22} = 5.48$, $L_{23} = 11.7$, $L_{24} = 11.51$, $L_{31} = 11.25$, $L_{32} = 11$, $L_{33} = 6$, $L_{34} = 11.7$, $L_{41} = 17$, $L_{42} = 26.5$, $L_{43} = 17$, $L_2 = 52$, $L_3 = 26.3$, $L_s = 26$, $W_1 = 0.58$, $W_2 = 1.5$, $W_3 = 0.5$,$W_4 = 0.5$, $W_c = 0.24$, $W_s = 1.6$, and $d = 0.6$ (unit: in millimeters). $R = 50\ \Omega$].

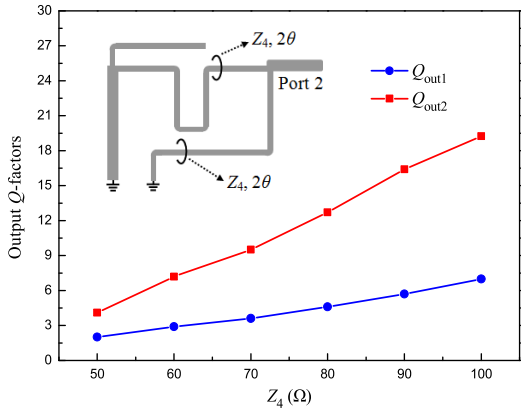

Fig. 8. Extracted output Q-factors of Prototype I versus Z_4.

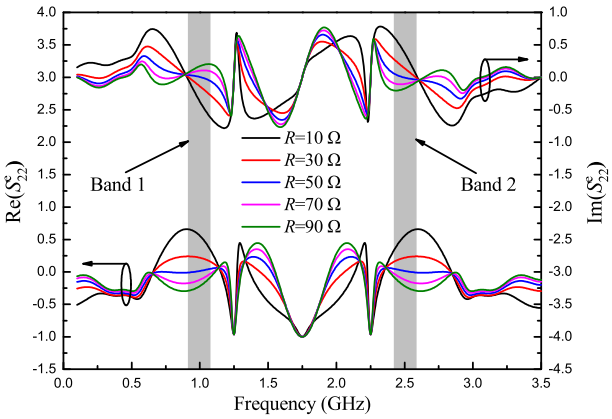

Fig. 9. Simulated $\mathrm{Re}(S_{22}^e)$ and $\mathrm{Im}(S_{22}^e)$ of Prototype I with varied R.

Fig. 7 delineates the realized circuit layout of Prototype I, and it is designed with central frequencies of 1.0 and 2.5 GHz, 0.043 dB ripple level, $\mathrm{FBW}_1 = 17.4\%$, and FBW2 = 7% in DM response. Based on these prescribed specifications, the type A dual-band admittance inverter is applied in the design, and the normalized element values for a second-order Chebyshev low-pass prototype filter are given as: $g_0 = 1$, $g_1 = 0.6648$, $g_2 = 0.5445$, and $g_3 = 1.221$. In accordance with the design procedure in Section II, $Z_c = 105\ \Omega$ and $Z_d = 367\ \Omega$ are first calculated to satisfy the required FBWs with $Z_3 = 70\ \Omega$. Then, $Z_1 = 75.6\ \Omega$ is determined to meet the

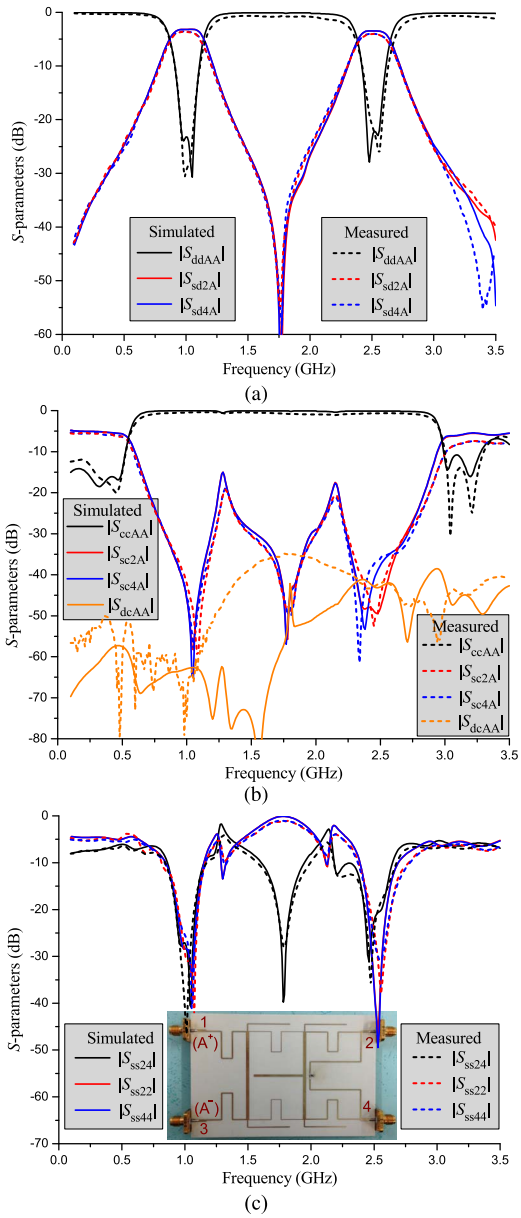

Fig. 10. Simulated and measured results of Prototype I. (a) DM responses. (b) CM responses. (c) Single-ended port responses.

input quality factors $Q_{\mathrm{in1}} = 3.82$, $Q_{\mathrm{in2}} = 9.55$. Fig. 8 depicts the extracted output Q-factors using the method in [35] under different impedance values of Z_4. Thus, the selection of $Z_4 = 71\ \Omega$ can give us the desired two values simultaneously as far as possible. With the aim of improving the in-band CM rejection, $Z_s = 35\ \Omega$ is selected accordingly. Fig. 9 plots different $\mathrm{Re}(S_{22}^e)$ and $\mathrm{Im}(S_{22}^e)$ with varied R, which indicates that the resistor with $R = 50\ \Omega$ can promise good in-band port matching and isolation in the design.

Final physical dimensions are provided in Fig. 7. The overall size of the fabricated circuit displayed in the inset of Fig. 10(c) is about $0.39\lambda_g \times 0.53\lambda_g$, where λ_g is the guided wavelength at 1.0 GHz. Simulated and measured results, portrayed in Fig. 10, are in good agreement with each other. As shown in Fig. 10(a), Prototype I exhibits two DM operating frequencies at 1.0 and 2.5 GHz with 1-dB FBWs of 21.3% and 8.6%. The measured in-band DM return losses for two

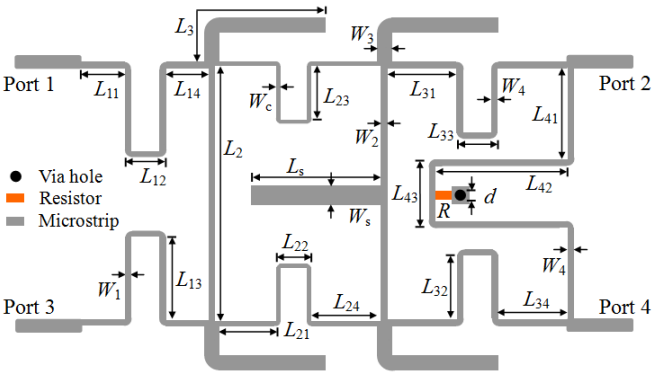

Fig. 11. Layout of Prototype II with dimensions included. [L_{11} = 7.55, L_{12} = 6.22, L_{13} = 15, L_{14} = 7.21, L_{21} = 10.5, L_{22} = 5.4, L_{23} = 13.2, L_{24} = 11, L_{31} = 12.8, L_{32} = 10, L_{33} = 5.9, L_{34} = 12.9, L_{41} = 17, L_{42} = 26, L_{43} = 17.3, L_2 = 52, L_3 = 26.6, L_s = 25.5, W_1 = 0.61, W_2 = 0.68, W_3 = 1.6,W_4 = 0.45, W_c = 0.2, W_s = 3.2, and d = 0.6 (unit: in millimeters). R = 60 Ω].

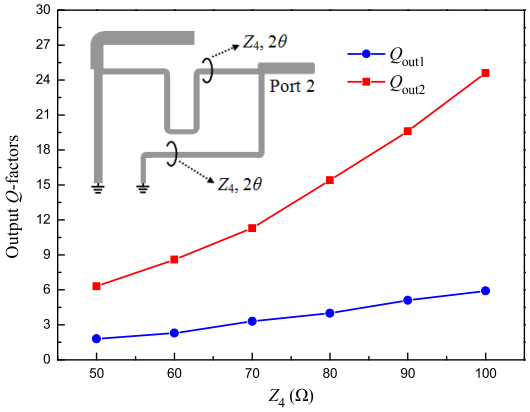

Fig. 12. Extracted output Q-factors of Prototype II for both two passbands versus the impedance Z_4.

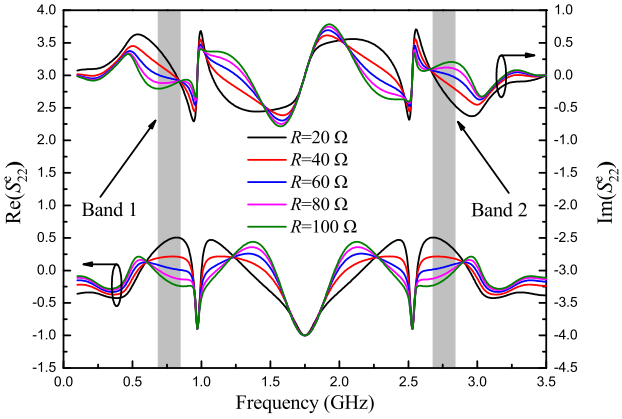

Fig. 13. Simulated Re(S^e_{22}) and Im(S^e_{22}) of Prototype II with varied R.

passbands are better than 25 and 22 dB, while the insertion losses at 1.0 and 2.5 GHz are 3.6 and 3.9 dB, respectively. From Fig. 10(b), the CM suppression is well enhanced to 35 dB in both of the two DM operation passbands with the help of two extra transmission zeros. In addition, the mode conversion of balanced port A, i.e., S_{dcAA}, is better than 40 dB over both passbands. Moreover, return losses of two unbalanced output ports are both better than 24 dB, and the tested isolations are greater than 21 dB within two whole passbands as indicated in Fig. 10(c).

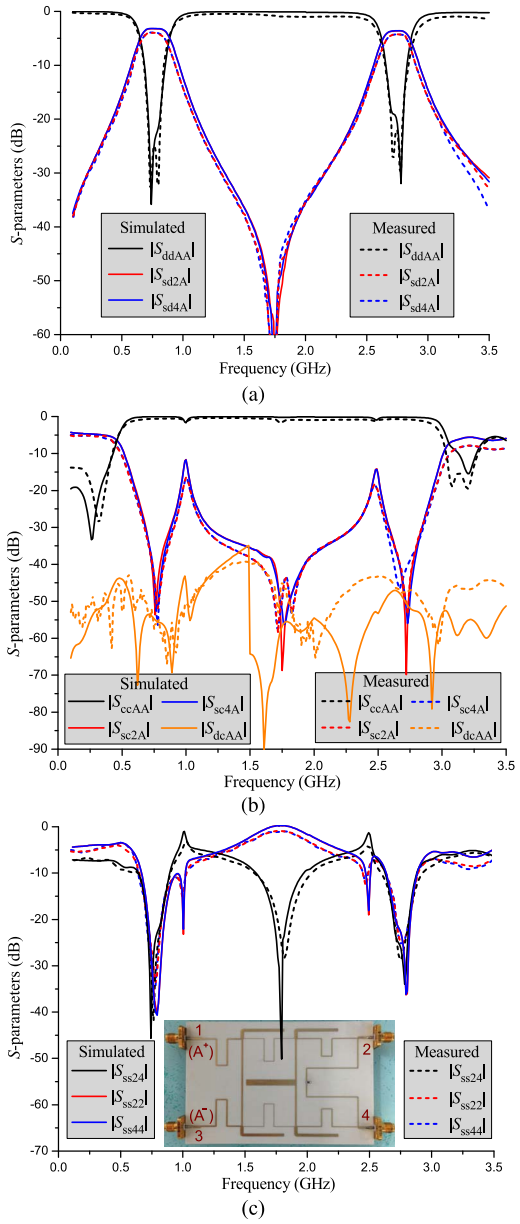

Fig. 14. Simulated and measured results of Prototype II. (a) DM responses. (b) CM responses. (c) Single-ended port responses.

As compared with Prototype I, the Prototype II balanced-to-unbalanced dual-band filtering power divider, with the increased frequency ratio as k = 3.62 is proposed as shown in Fig. 11. Alternatively, Prototype II is designed with two DM central frequencies of 0.76 and 2.75 GHz, two FBWs of 19% and 5.3% with 0.043-dB ripple level. Different from Prototype I, type B dual-band J-inverter is used herein for the condition of $k > 3$ in Prototype II. Corresponding design parameters Z_c = 114 Ω, Z_d = 434 Ω, Z_1 = 78 Ω, and Z_s = 20 Ω are derived with Z_3 = 40 Ω following the design procedure. In addition, Z_4 = 79 Ω are properly selected for the extracted output quality factors from Fig. 12. As for the isolated resistor, it is chosen with R = 60 Ω herein based on the variation curves of Re(S^e_{22}) and Im(S^e_{22}) in Fig. 13. Practical design geometric parameters are denoted in Fig. 11 with the overall size of $0.3\lambda_g \times 0.4\lambda_g$, where λ_g is the guided wavelength at 0.76 GHz.

TABLE I
PERFORMANCE COMPARISONS WITH OTHER REPORTED BALANCED-TYPE FILTERING POWER DIVIDERS

Ref.	Type	f_0 or (f_1, f_2), Frequency Ratio k	DM Bandwidth ABW	DM Bandwidth FBW	DM Insertion Loss	In-Band CM Suppression	In-Band Isolation	Output Port Return Loss	Dimension ($\lambda_g \times \lambda_g$)
[16]-I	Single-Band BTB FPD	2.02 GHz	170 MHz	8.4%	3.81 dB	>20 dB	>20 dB	>13 dB	0.87×0.97
[17]	Single-Band BTB FPD	2.385 GHz	131 MHz	5.5%	6.6 dB	>19 dB	>9.1 dB	/	0.28×0.30
[25]-II	Single-Band BTUB FPD	1.88 GHz	95 MHz	5.0%	3.7 dB	>21 dB	>15 dB	/	0.30×1.10
[26]-I	Single-Band BTUB FPD	2.0 GHz	1.61 GHz	80.5%	3.4 dB	>10 dB	>15 dB	>15 dB	0.26×0.52
[27]	Dual-Band BTB FPD	1.8, 2.4 GHz k =1.33	396, 624 MHz	22%, 26%	3.2, 4.1 dB	>30 dB	/	/	0.34×0.45
[28]	Dual-Band BTUB FPD	2.82, 3.2 GHz k =1.13	79, 99 MHz	2.8%, 3.1%	/	>15 dB	>15 dB	>18 dB	/
Prototype I	**Dual-Band BTUB FPD**	**1.0, 2.5 GHz k =2.5**	**213, 215 MHz**	**21.3%, 8.6%**	**3.6, 3.9 dB**	**>35 dB**	**>21 dB**	**>24 dB**	**0.39×0.53**
Prototype II	**Dual-Band BTUB FPD**	**0.76, 2.75 GHz k =3.62**	**168, 165 MHz**	**22.4%, 6%**	**3.8, 4.1 dB**	**>34 dB**	**>24 dB**	**>22 dB**	**0.30×0.40**

BTB FPD: Balanced-to-balanced filtering power divider; BTUB FPD: Balanced-to-unbalanced filtering power divider; λ_g: Guided wavelength at the central frequency f_0 or the first frequency band f_1; ABW: Absolute bandwidth; FBW: Fractional bandwidth.

Fig. 14 depicts the final results of simulation and experiment, from which two DM passbands are centered at 0.76 and 2.75 GHz with 1-dB FBWs of 22.4% and 6%. The tested insertion losses at two central frequencies are 3.8 and 4.1 dB, and the return losses are greater than 25 and 22 dB inside each passband for the DM operation. From Fig. 14(b), CM rejection levels to unbalanced ports are greatly improved to approximately 34 dB across both passbands as expected, and the conversion between DM to CM at balanced port A is better than 45 dB for both passbands. In addition, in Fig. 14(c), the unbalanced ports return losses are better than 22 dB, and the isolation is larger than 24 dB within two DM passband regions.

A detailed comparison of the proposed designs with other balanced-type filtering power dividers is provided in Table I. It can be observed from Table I that the proposed balanced-to-unbalanced filtering power dividers provide dual working passbands with controllable frequency ratio and DM bandwidth. Moreover, compared with other counterparts, both our proposals show very nice in-band performances in terms of the port-to-port isolation, the port matching, and especially the CM suppression.

IV. CONCLUSION

In this paper, a new balanced-to-unbalanced filtering power divider design with dual operation passbands has been proposed. Generalized mixed-mode S-parameters are initially derived to reveal the operation principle. Not only has the DM dual-band filtering response been illustrated with theoretical formulations but also the CM signals across dual passbands have been significantly rejected with resorting to two extra transmission zeros engendered by the added open-ended stub. In addition, nice in-band isolation and port matching are easily achieved by means of one grounded resistor. Consequently, two prototypes with different frequency ratios are presented following the design procedure, and the final results from both simulation and experiment are in good agreement with each other, well corroborating our design approach. In a nutshell, the developed dual-band balanced-to-unbalanced filtering power divider can be served as a good candidate in balanced or differential circuits and systems due to its high performance.

REFERENCES

[1] D.-J. Eom, S. Kahng, B. Lee, C. Woo, and H. Lee, "Wide-band power divider miniaturized by combining CRLH ZOR bandpass filters," in *Proc. Asia–Pacific Microw. Conf.*, Dec. 2012, pp. 541–543.

[2] P.-H. Deng and Y.-T. Chen, "New Wilkinson power dividers and their integration applications to four-way and filtering dividers," *IEEE Trans. Compon., Packag., Manuf. Technol.*, vol. 4, no. 11, pp. 1828–1837, Nov. 2014.

[3] K. X. Wang, X. Y. Zhang, and B.-J. Hu, "Gysel power divider with arbitrary power ratios and filtering responses using coupling structure," *IEEE Trans. Microw. Theory Techn.*, vol. 62, no. 3, pp. 431–440, Mar. 2014.

[4] Y. C. Li, Q. Xue, and X. Y. Zhang, "Single- and dual-band power dividers integrated with bandpass filters," *IEEE Trans. Microw. Theory Techn.*, vol. 61, no. 1, pp. 69–76, Jan. 2013.

[5] W.-M. Chau, K.-W. Hsu, and W.-H. Tu, "Filter-based Wilkinson power divider," *IEEE Microw. Wireless Compon. Lett.*, vol. 24, no. 4, pp. 239–241, Apr. 2014.

[6] T.-S. Dang, C.-W. Kim, and S.-W. Yoon, "Ultra-Wideband power divider using three parallel-coupled lines and one shunt stub," *Electron. Lett.*, vol. 50, no. 2, pp. 95–96, Jan. 2014.

[7] C. T. Cai, J. P. Wang, Y. J. Deng, and J.-L. Li, "Design of compact dual-mode dual-band filtering power divider with high selectivity," *Electron. Lett.*, vol. 51, no. 22, pp. 1795–1796, Oct. 2015.

[8] G. Zhang, J. P. Wang, L. Zhu, and W. Wu, "Dual-band filtering power divider with high selectivity and good isolation," *IEEE Microw. Wireless Compon. Lett.*, vol. 26, no. 10, pp. 774–776, Oct. 2016.

[9] T. B. Lim and L. Zhu, "A differential-mode wideband bandpass filter on microstrip line for UWB application," *IEEE Microw. Wireless Compon. Lett.*, vol. 19, no. 10, pp. 632–634, Oct. 2009.

[10] Y. G. Zhou, H.-W. Deng, and Y. J. Zhao, "Compact balanced-to-balanced microstrip diplexer with high isolation and common-mode suppression," *IEEE Microw. Wireless Compon. Lett.*, vol. 24, no. 3, pp. 143–145, Mar. 2014.

[11] L.-S. Wu, B. Xia, J. F. Mao, and W.-Y. Yin, "A half-mode substrate integrated waveguide ring for two-way power division of balanced circuit," *IEEE Microw. Wireless Compon. Lett.*, vol. 22, no. 7, pp. 333–335, Jul. 2012.

[12] B. Xia, L.-S. Wu, and J. F. Mao, "A new balanced-to-balanced power divider/combiner," *IEEE Trans. Microw. Theory Techn.*, vol. 60, no. 9, pp. 2791–2798, Sep. 2012.

[13] B. Xia, L.-S. Wu, S.-W. Ren, and J.-F. Mao, "A balanced-to-balanced power divider with arbitrary power division," *IEEE Trans. Microw. Theory Techn.*, vol. 61, no. 8, pp. 2831–2840, Aug. 2013.

[14] J. Shi, J. Wang, K. Xu, J.-X. Chen, and W. Liu, "A balanced-to-balanced power divider with wide bandwidth," *IEEE Microw. Wireless Compon. Lett.*, vol. 25, no. 9, pp. 573–575, Sep. 2015.

[15] W. Feng, C. Y. Zhao, W. Che, and Q. Xue, "Wideband balanced network with high isolation using double-sided parallel-strip line," *IEEE Trans. Microw. Theory Techn.*, vol. 63, no. 12, pp. 4013–4018, Dec. 2015.

[16] L.-S. Wu, Y.-X. Guo, and J.-F. Mao, "Balanced-to-balanced Gysel power divider with bandpass filtering response," *IEEE Trans. Microw. Theory Techn.*, vol. 61, no. 12, pp. 4052–4062, Dec. 2013.

[17] C.-L. Huang and Y.-H. Pang, "Filtering power divider for differential input and output signals," in *Proc. Asia-Pacific Microw. Conf.*, Nov. 2013, pp. 369–371.

[18] H. Chu, J.-X. Chen, and Y.-X. Guo, "Substrate integrated waveguide differential filtering power divider with good common-mode suppression and high selectivity," *Electron. Lett.*, vol. 51, no. 25, pp. 2115–2117, Dec. 2015.

[19] L.-S. Wu, Y.-X. Guo, L.-F. Qiu, and J.-F. Mao, "A new balanced-to-single-ended (BTSE) power divider," in *Proc. IEEE Int. Wireless Symp.*, Mar. 2014, pp. 1–4.

[20] W. W. Zhang, Y. L. Wu, Y. A. Liu, F. M. Ghannouchi, and A. Hasan, "A wideband balanced-to-unbalanced coupled-line power divider," *IEEE Microw. Wireless Compon. Lett.*, vol. 26, no. 6, pp. 410–412, Jun. 2016.

[21] A. N. Yadav and R. Bhattacharjee, "Balanced to unbalanced power divider with arbitrary power ratio," *IEEE Microw. Wireless Compon. Lett.*, vol. 26, no. 11, pp. 885–887, Nov. 2016.

[22] J. Shi, J. P. Lu, K. Xu, and J.-X. Chen, "A coupled-line balanced-to-single-ended out-of-phase power divider with enhanced bandwidth," *IEEE Trans. Microw. Theory Techn.*, vol. 65, no. 2, pp. 459–466, Feb. 2017.

[23] W. W. Zhang *et al.*, "Planar miniaturized balanced-to-single-ended power divider based on composite left- and right-handed transmission lines," *IEEE Microw. Wireless Compon. Lett.*, vol. 27, no. 3, pp. 242–244, Mar. 2017.

[24] W. J. Feng, M. L. Hong, M. Z. Xun, and W. Q. Che, "A novel wideband balanced-to-unbalanced power divider using symmetrical transmission lines," *IEEE Microw. Wireless Compon. Lett.*, vol. 27, no. 4, pp. 338–340, Apr. 2017.

[25] K. Xu, J. Shi, L. L. Lin, and J.-X. Chen, "A balanced-to-unbalanced microstrip power divider with filtering function," *IEEE Trans. Microw. Theory Techn.*, vol. 63, no. 8, pp. 2561–2569, Aug. 2015.

[26] X. Gao, W. J. Feng, W. Q. Che, and Q. Xue, "Wideband balanced-to-unbalanced filtering power dividers based on coupled lines," *IEEE Trans. Microw. Theory Techn.*, vol. 65, no. 1, pp. 86–95, Jan. 2017.

[27] P. Vélez, M. Durán-Sindreu, A. Fernández-Prieto, J. Bonache, F. Medina, and F. Martin, "Compact dual-band differential power splitter with common-mode suppression and filtering capability based on differential-mode composite right/left-handed transmission-line metamaterials," *IEEE Antennas Wireless Propag. Lett.*, vol. 13, pp. 536–539, 2014.

[28] W. J. Feng, M. L. Hong, and W. Q. Che, "Dual-band balanced-to-unbalanced filtering power divider by coupled ring resonators," *Electron. Lett.*, vol. 52, no. 22, pp. 1862–1864, Oct. 2016.

[29] W. R. Eisenstadt, R. Stengel, and B. M. Thompson, *Microwave Differential Circuit Design Using Mixed-Mode S-Parameters*. Boston, MA, USA: Artech House, 2006.

[30] D. E. Bockelman and W. R. Eisenstadt, "Combined differential and common-mode scattering parameters: Theory and simulation," *IEEE Trans. Microw. Theory Techn.*, vol. 43, no. 7, pp. 1530–1539, Jul. 1995.

[31] M. Roberg and C. Campbell, "A novel even & odd-mode symmetric circuit decomposition method," in *Proc. IEEE Compound Semicond. Integr. Circuit Symp.*, Oct. 2013, pp. 1–4.

[32] M. Sagawa, M. Makimoto, and S. Yamashita, "Geometrical structures and fundamental characteristics of microwave stepped-impedance resonators," *IEEE Trans. Microw. Theory Techn.*, vol. 45, no. 7, pp. 1078–1085, Jul. 1997.

[33] G. L. Matthaei, E. M. T. Jones, and L. Young, *Microwave Filters, Impedance-Matching Networks, and Coupling Structures*. Norwood, MA, USA: Artech House, 1980.

[34] C. Monzon, "A small dual-frequency transformer in two sections," *IEEE Trans. Microw. Theory Techn.*, vol. 51, no. 4, pp. 1157–1161, Apr. 2003.

[35] J.-S. Hong and M. J. Lancaster, *Microstrip Filters for RF/Microwave Applications*. New York, NY, USA: Wiley, 2001.

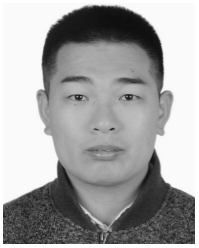

Feng Huang received the B.S. degree in electronic and information engineering from Nantong University, Nantong, China, in 2013. He is currently pursuing the Ph.D. degree in electromagnetic field and microwave technology at the Nanjing University of Science and Technology, Nanjing, China.

He is currently a Visiting Scholar with the School of Engineering and Physical Sciences, Heriot-Watt University, Edinburgh, U.K. His current research interests include microwave components, balanced circuit design, and functions integrated circuit design.

Jianpeng Wang received the Ph.D. degree from the University of Electronic Science and Technology of China, Chengdu, China, in 2007.

From 2005 to 2006, he was a Research Assistant with the Institute for Infocomm Research, Singapore. From 2010 to 2011, he was a Research Fellow with the School of Electrical and Electronic Engineering, Nanyang Technological University, Singapore. In 2013, he joined the School of Engineering and Physical Sciences, Heriot-Watt University, Edinburgh, U.K., as a Visiting Scholar. From 2014 to 2016, he was a Research Fellow with the Faculty of Science and Technology, University of Macau, Macau, China. He is currently an Associate Professor with the School of Electronic and Optical Engineering, Nanjing University of Science and Technology, Nanjing, China. He has authored or co-authored over 90 papers in international journals and conference proceedings. His current research interests include microwave circuits, antennas, and LTCC-based millimeter-wave circuits.

Dr. Wang has been an Associate Editor of *IET Electronics Letters* since 2015.

Jiasheng Hong (M'94–SM'05–F'12) received the D.Phil. degree in engineering science from the University of Oxford, Oxford, U.K., in 1994. His doctoral dissertation was focused on electromagnetic (EM) theory and applications.

In 1994, he joined the University of Birmingham, Birmingham, U.K., where he was involved with microwave applications of high-temperature superconductors, EM modeling, and circuit optimization. In 2001, he joined the Department of Electrical, Electronic and Computer Engineering, Heriot-Watt University, Edinburgh, U.K., where he is currently a Professor leading a team on research into advanced RF/microwave device technologies. He has authored or co-authored over 200 journal and conference papers and 2 books, *Microstrip Filters for RF/Microwave Applications* (Wiley, first edition, 2001, and second edition, 2011) and *RF and Microwave Coupled-Line Circuits* (Artech House, second edition, 2007). His current research interests include RF/microwave devices, such as antennas and filters, for wireless communications and radar systems, as well as novel material and device technologies including multilayer circuit technologies using package materials such as liquid crystal polymer, RF MEMS, and ferroelectric and high-temperature superconducting devices.

Wen Wu (SM'10) received the Ph.D. degree in electromagnetic field and microwave technology from Southeast University, Nanjing, China, in 1997.

He is currently a Professor with the School of Electronic Engineering and Optoelectronic Technology, Nanjing University of Science and Technology, Nanjing, where he is currently an Associate Director with the Ministerial Key Laboratory of JGMT. He has authored or co-authored over 240 journal and conference papers. He holds 14 patents. His current research interests include microwave- and millimeter-wave theories and technologies, microwave and millimeter-wave detection, and multimode compound detection.

Dr. Wu was a six-time recipient of the Ministerial and Provincial-Level Science and Technology Award.